List of Changes and Responses for Ocean Science Discussion (OS-2020-91)

Interactive comment on
"Zonal Current Characteristics in the Southeastern Tropical Indian Ocean (SETIO)"

Thank you for your time and effort in reviewing our paper, and for providing the valuable suggestions, comments, and corrections, which helped make our manuscript stronger. We have modified the manuscript based on the Reviewer's suggestions and hope that the revision adequately addressed the Reviewer's concerns, so that the revised manuscript will be suitable for publication.

Anonymous Referee #1
Received and published: 3 December 2020

This study investigates the variability of zonal current in the Southeastern Tropical Indian Ocean using HYCOM simulations. The authors described the simulated features of zonal currents in the SJC and ITF/SEC region and examined the intraseasonal to interannual variability of zonal currents in this region. Some interesting results are reported, but a major revision is needed. The major problem with this manuscript is the methodology the authors used. Please see my following comments for details.

Major comments:

1. The authors described the simulated "Vertical structure of zonal current" along transects A, B and C in sections 3.2.1, 3.2.2 and 3.2.3. However, it does not make sense to discuss the "zonal current" along a southeast-northwest section like transects A and B, and especially when there is no clear mean currents along the transects. The meridional components of velocity in the transects A and B are obviously important as shown in Figures 1a and 2. I suggest that the authors use meridional sections (e.g., AEJ-BEJ-CEJ).

Thank you for your suggestions. We have revised the description of "Vertical structure of zonal current" by using meridional sections (East Java: AEJ-BEJ-CEJ; West Java: AWJ-BWJ-CWJ; and Sumatra: ASM-BSM-CSM). In addition, the revision can also be seen at the end of this response for details.

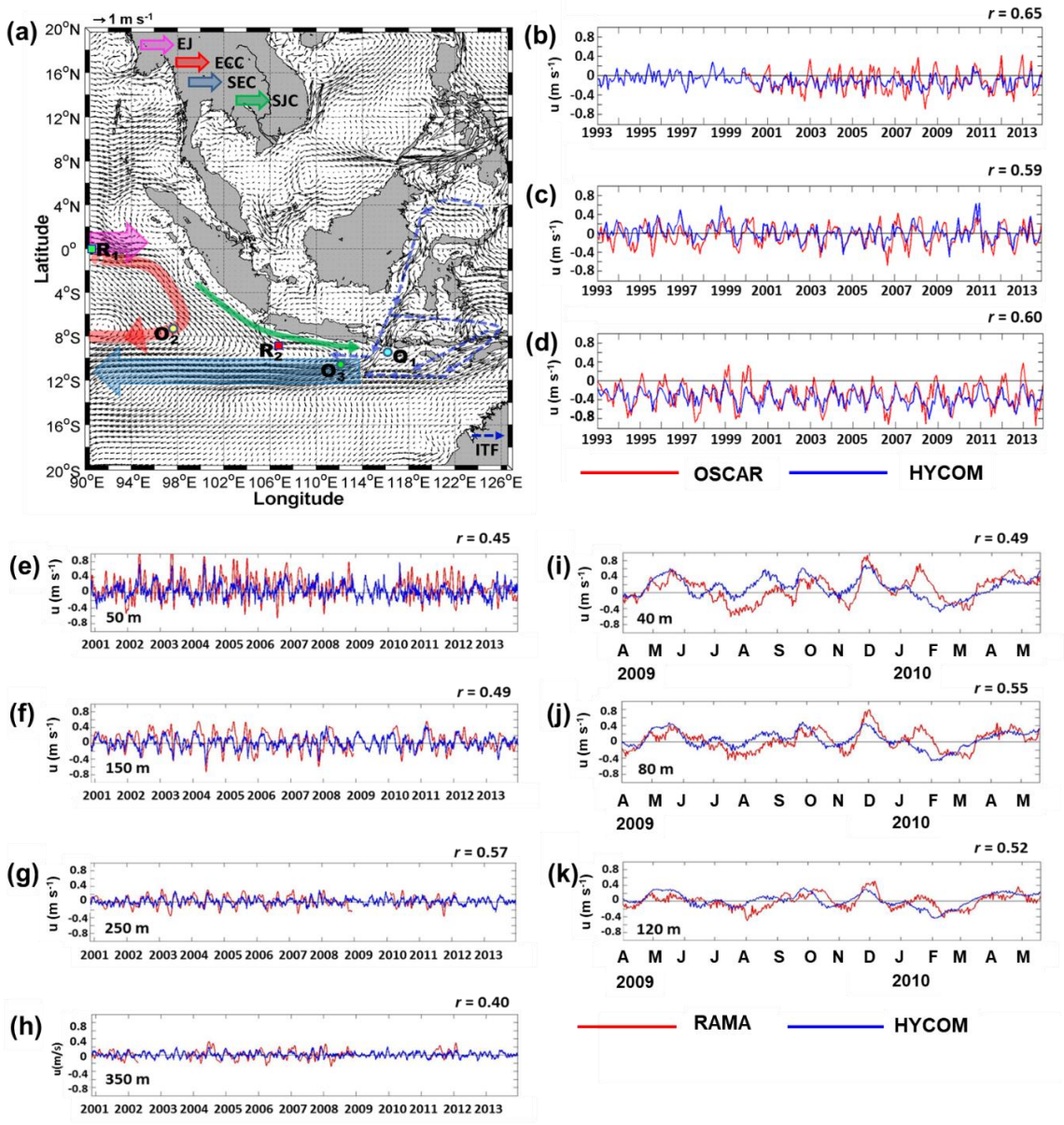

Figure 1. Validation of HYCOM zonal currents with OSCAR and RAMA datasets: (a) Locations of validation points: Points O1 (8ºS, 116ºE), O2 (7ºS, 98ºE), and O3 (11.5ºS, 113ºE) for the OSCAR data, while R1 (0ºS, 90ºE) and R2 (8.5ºS, 106.75ºE) for the RAMA data. (b)-(d) Time series of the zonal currents observed by the HYCOM (blue lines) and the OSCAR (red lines) at a depth of 0.5 m at point O1, O2, and O3, respectively. Meanwhile (e)-(h) are the time series of zonal currents observed by the HYCOM (blue lines) and the moored RAMA (red lines) at point R1 at depths of 50, 150, 250, and 350 m, sequentially. Meanwhile, (i)-(k) are the same as (e)-(h), except for point R2 and depths of 40, 80, and 120 m, respectively. In the Figures 1e-h (point R1), a monthly low-pass filter has been applied before plotting.

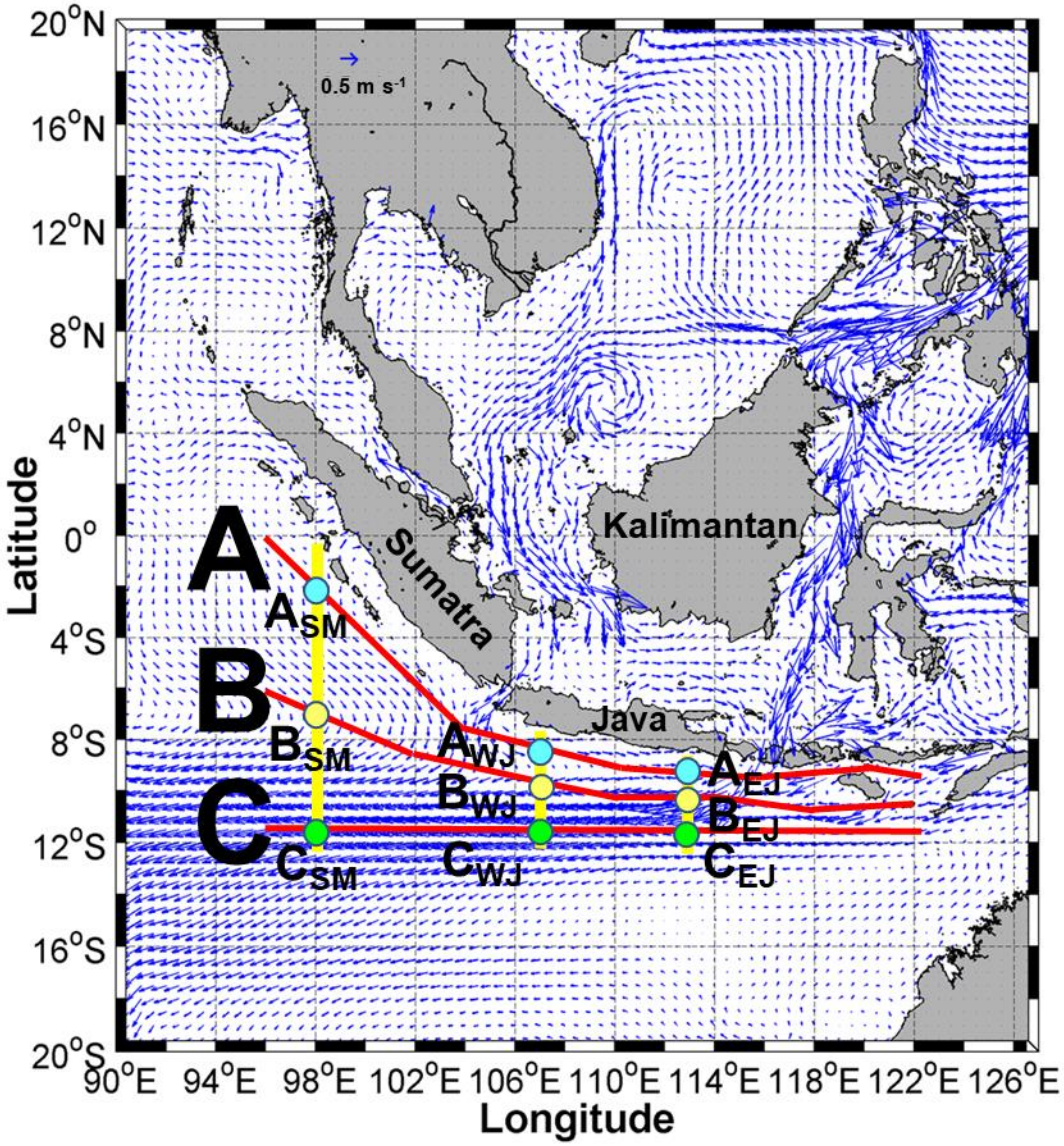

Figure 2. The area of study interest in the SETIO region adjacent to the Sumatra-Java southern coasts. The blue arrows show climatological (yearly mean) surface (1 m) current field over 64 years from 1950 to 2013. Yellow lines are the meridional sections along the three longitudes (98°E, 107°E, and 113°E), while red lines are the three selected transects: A, B, and C. Green, yellow, and cyan circles are the locations in which the zonal currents are analysed, namely points ASM, AWJ, AEJ (on the Transect A); points BSM, BWJ, and BEJ (on the Transect B); and points CSM, CWJ, and CEJ (on the Transect C). The subscripts SM, WJ, and EJ denote regions which close to Sumatra, West Java, and East Java.

2. The authors used EOF analysis to the zonal velocity at selected points, e.g., AWJ, to investigate the variability of zonal currents SJC, ITF and SEC. But unfortunately, the zonal component of velocity at a selected point is obviously not the currents they aimed to study, just considering that the zonal currents are not steady and usually swing horizontally and that the meridional components of the velocity are non-negligible for these coastal currents.

As I said, it might be good to examine the EOF modes of zonal currents across the meridional sections.

Thank you for your valuable suggestions. We have added examination of the EOF modes of zonal currents across the meridional sections, namely sections East Java (EJ), West Java (WJ), and Sumatra (SM), as follows:

EOF analysis gives vertical mode structures (spatial mode) and their normalized temporal mode variabilities relative to the mean which influence zonal current variability in the study area. Before performing the EOF analysis, the average value of the current data has been removed (solid black lines in the Figs. 3a-r). To further analyze the zonal current characteristics in the nearshore and offshore areas, and the transition region between them, we examined the EOF modes of zonal current across the three meridional sections (EJ, WJ, and SM). In this paper, we only considered the first mode of EOF (EOF1) analysis since it is associated with the largest percent of the variance. Figure 4 shows vertical structures and their associated temporal variability of EOF1 of zonal currents along the meridional sections. Here, as an example, the temporal variability is only shown for the last eight-year period of the EOF1 (2006 to 2013). It can be clearly seen that remarkable features of zonal currents are revealed between nearshore and offshore areas as well as in the three meridional sections (Fig. 4).

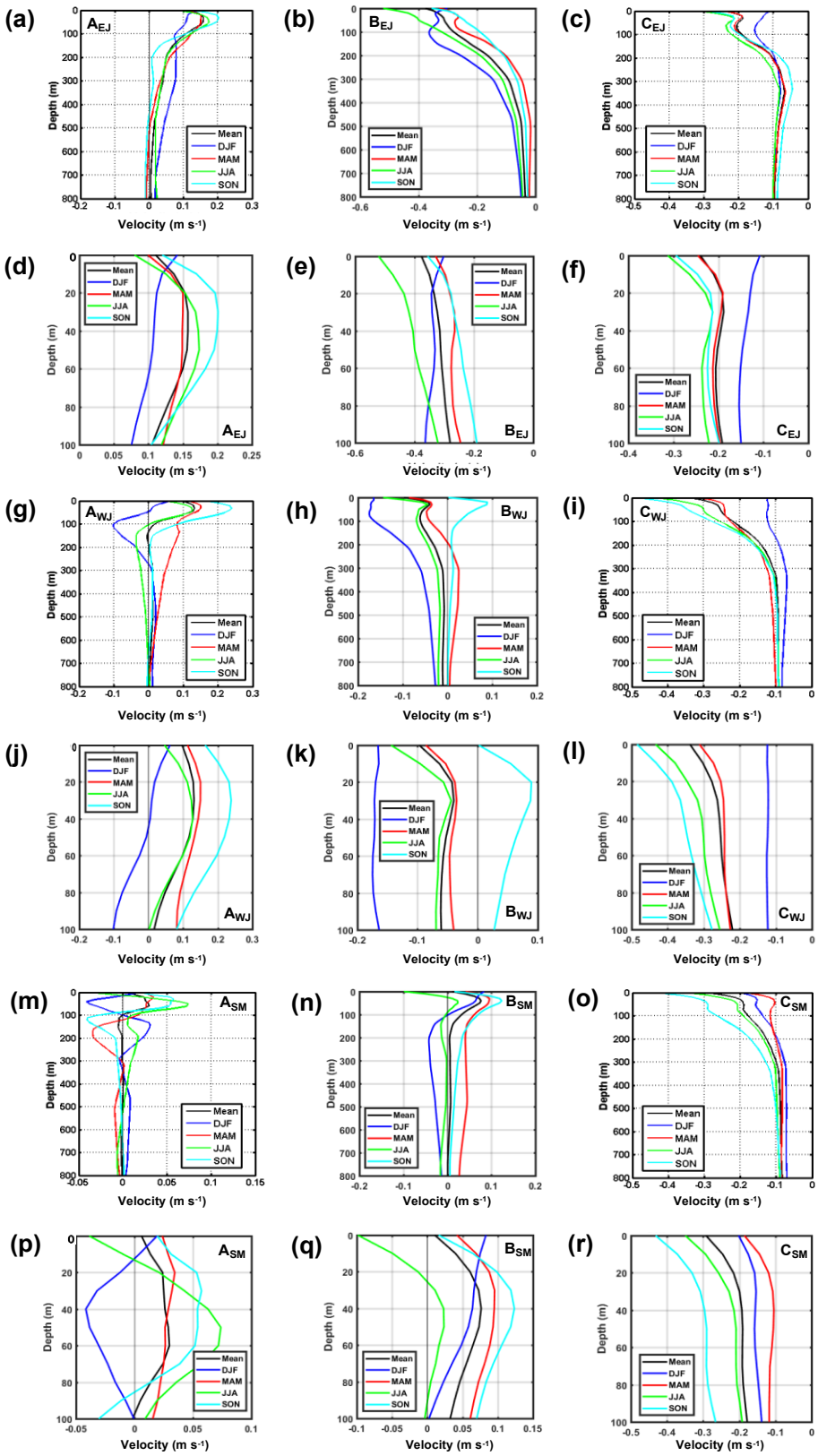

Figure 3. Mean and seasonal depth profiles of zonal current velocity derived from the HYCOM simulation results for the period of 1950 through 2013, at points: (a) AEJ, (b) BEJ, (c) CEJ, (g) AWJ, (h) BWJ, (i) CWJ, (m) ASM, (n) BSM, and (o) CSM. Meanwhile, (d)-(f), (j)-(l), and (p)-(r) are the same as (a)-(c), (g)-(i), and (m)-(o), respectively, except for depths of 0-100 m.

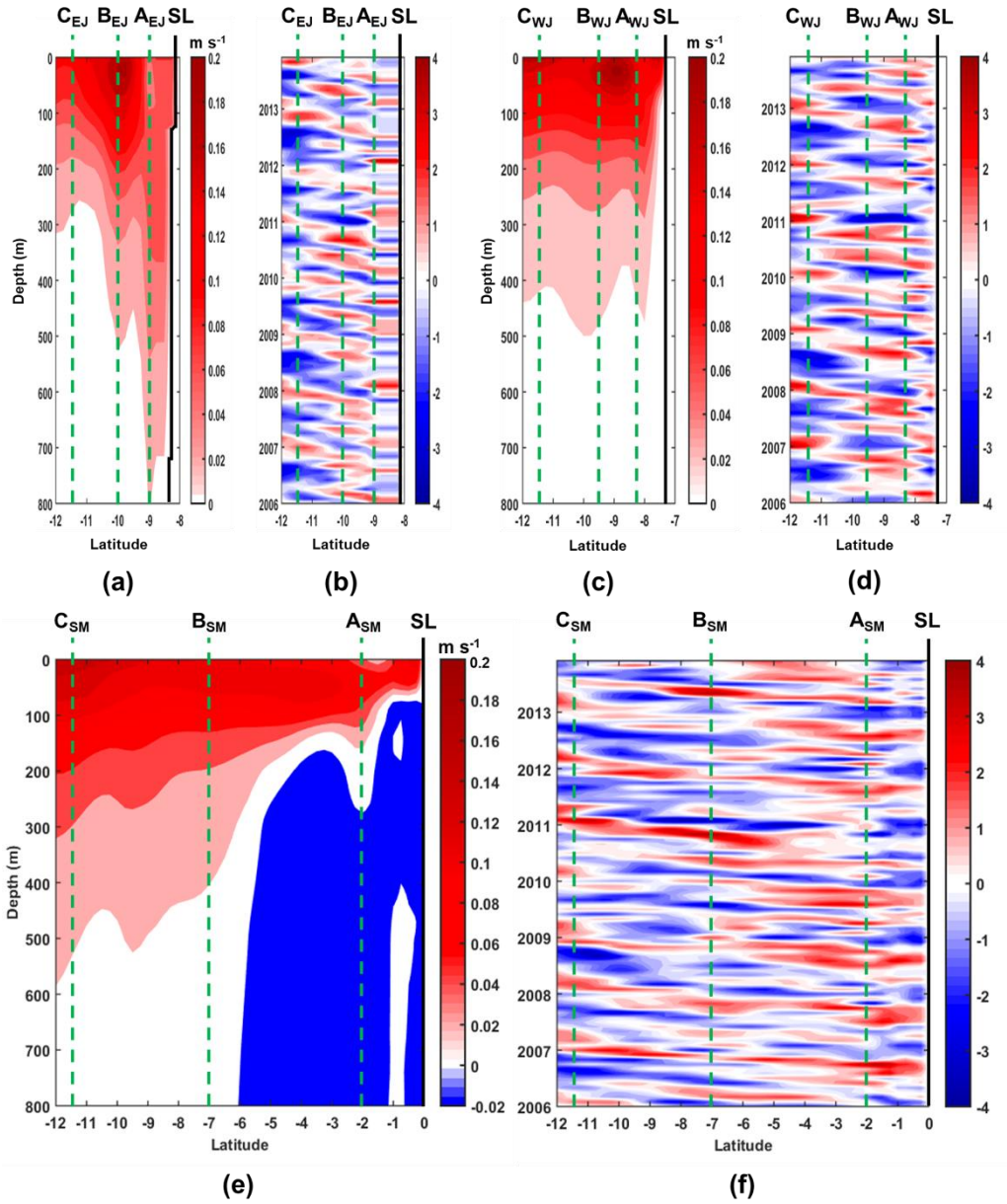

Figure 4. Vertical structures (a, c, and e) and their associated temporal variability of EOF1 (b, d, and f) of zonal currents along the three meridional sections: EJ (a and b), WJ (c and d), and SM (e and f). In this case, the temporal variability is shown for the last eight-year period of the EOF1. Positive (negative) values of the vertical structure indicate eastward (westward). Meanwhile, green dash lines indicate latitudes of the nine analyzed points and SL is shoreline.

In general, temporal mode of EOF1 of zonal currents across each meridional section shows intraseasonal and semiannual variabilities both in the nearshore and transition regions, whereas annual and interannual variations exist in the offshore area. However, the vertical structures of EOF1 in each section are quite different. In the nearshore area of Section EJ (Fig. 4a), the vertical structure of EOF1 is characterized by one-layer flow with a gradual decrease in speed from the surface to 800 m depth, whereas in the transition and the offshore regions the flow velocities decrease more rapidly from the surface to nearly zero at depths of about 500 m and 300 m, respectively. Meanwhile, in Section WJ (Fig. 4b), the vertical structure of EOF1 is also

characterized by one-layer flow in which the unidirectional vertical structure gradually decreases from the surface to a depth of about 450 m in all areas. In contrast, a different vertical structure of EOF1 appears in Section SM (Fig. 4e). In this section, the vertical structure is characterized by two-layer flow in the nearshore and transition regions with the changeover between the two types of flow occurring at a depth of about 100 m and 200 m, respectively. In addition, in the offshore area of Section SM, the vertical structure of EOF1 displays unidirectional flow from the surface to a depth of ~500 m.

To examine the EOF modes of zonal currents in more detail, further analysis was performed at three points on each meridional transect, namely points A_{EJ}, B_{EJ}, and C_{EJ} (Transect EJ); points A_{WJ}, B_{WJ}, and C_{WJ} (Transect WJ); and points A_{SM}, B_{SM}, and C_{SM} (Transect SM). Table 1 displays dominant variances at those points. From the Table 1, the first three modes at each point already represent ≥ 95% of the total variance. In fact, the first two modes at each point (except at points A_{SM} and A_{EJ}) already represent ≥ 91% of the total variance.

Table 1. Dominant variances at the nine observation points.

Mode	**Variance (%)**								
	Section EJ			**Section WJ**			**Section SM**		
	A_{EJ}	**B_{EJ}**	**C_{EJ}**	**A_{WJ}**	**B_{WJ}**	**C_{WJ}**	**A_{SM}**	**B_{SM}**	**C_{SM}**
1	60	76	**72**	**58**	84	87	37	**64**	88
2	29	18	20	33	12	10	25	27	9
3	6	4	3	5			13	6	
4			2				10		
5							6		
6							4		
Total	**95**	**98**	**97**	**96**	**96**	**97**	**95**	**97**	**97**

In here, we only consider the first modes of EOF analysis for further analysis since their percent variances (except at point A_{SM}) are more than 50% of the total variance (Table 1). Since the temporal variability of the EOF1 contains more than one frequency (Figs. 4b, 4d, and 4f) and to find out what frequencies are dominant in the EOF1, it was then analyzed by using the EEMD method to decompose the signal. In this study, the EEMD analyses of currents are only presented at one point on each meridional transect, namely A_{WJ} (Transect WJ), B_{SM} (Transect SM), and C_{EJ} (Transect EJ). The A_{WJ}, B_{SM}, and C_{EJ} points were chosen to investigate SJC variability, interannual variability in the open SETIO, and SEC and ITF variabilities, respectively.

The EEMD analysis of the first temporal EOF mode provides 10 modes/signals in which the first signal of the EEMD result is the summation of the second to tenth signals, which is the same as the original EOF first temporal mode of zonal currents. Meanwhile, the second–sixth signals of the EEMD result vary from intraseasonal to interannual variabilities. The remaining signals of EEMD result show the long-term trend.

3. The authors used EEMD analysis to the EOF1 (PC1) as well, but I do not understand why the authors did this. The EOF1 itself represents a mode, which means an eigen-mode with an eigenperiod. Then, why an eigenmode could be further decomposed into various modes with various periods?

Thank you for the comments. We would like to clarify it.

EOF via singular value decomposition matrix of data decomposes into three new matrices which may be used to form the eigenvalues, eigenvectors, and eigenfunctions. The resulting eigenfunctions display the spatial patterns (in our case, the vertical patterns for mode-1 shown in Figs. 5a, 6a, 7a), while the eigenvectors (eigenperiod) show time varying amplitude for each mode (in our case, the eigenperiod for mode-1 shown in Figs. 5b, 6b, and 7b). The eigenvalues demonstrate the strength of each mode, with the first mode defines as being the mode associated with the largest eigenvalue, and hence the largest percent of the variance (Table 1).

To find out what frequencies are dominant in the eigenperiod of mode-1, one can apply Fourier transform of these time series (Figs. 5b, 6b, and 7b) by assuming that the time varying signal is linear and periodic. In here, we use time series analysis technique (EEMD) which is using Hilbert transform, that suitable not only for linear periodic time series, but also suitable for nonlinear and nonperiodic signals. For detailed technique, please refer to Huang et al., 1998. Our results are shown in Figs. 5d-h, 6d-h, and 7d-h.

We do hope this could clarify it. Thank you.

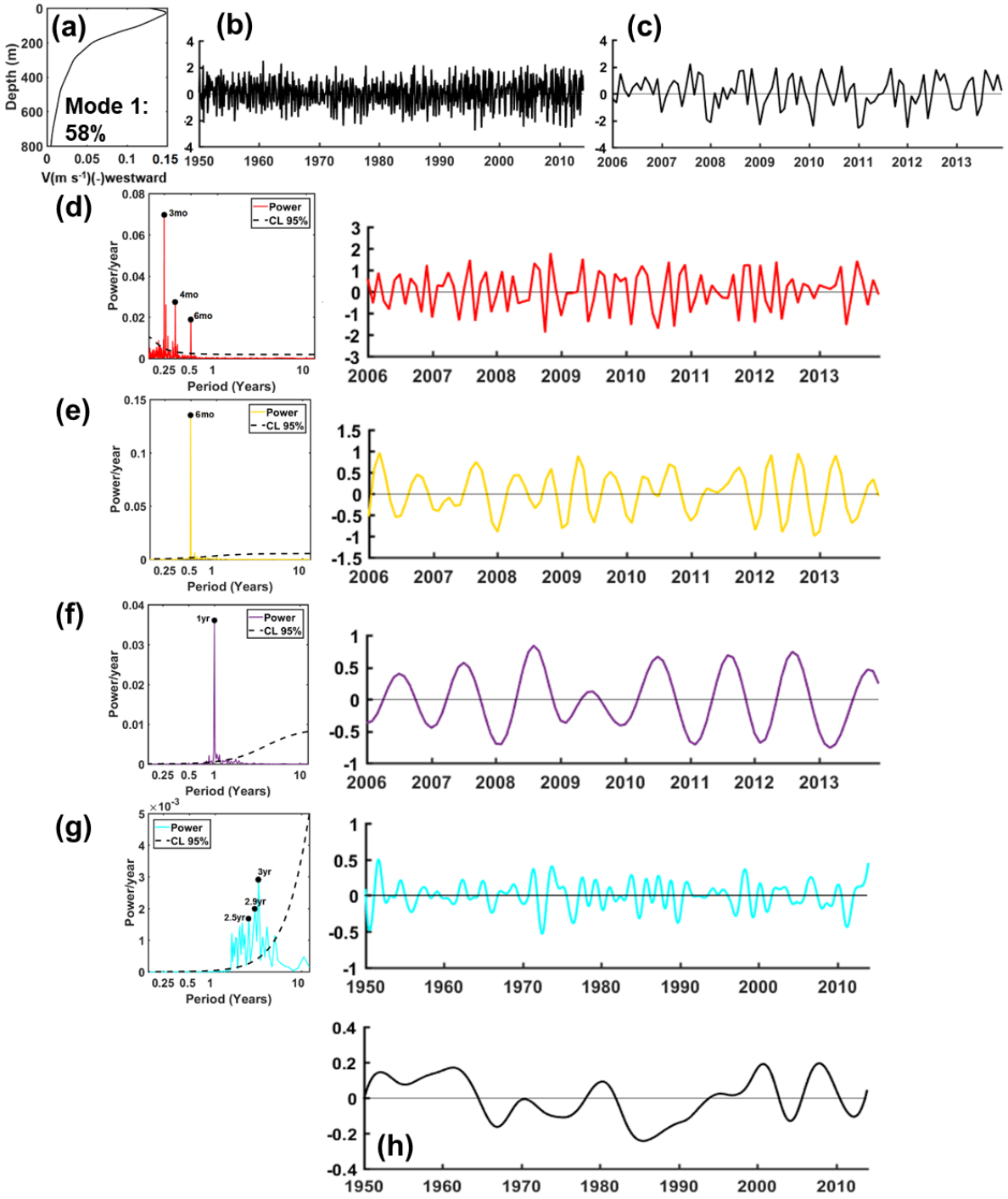

Figure 5. (a) Vertical structure and (b) its associated temporal variability of EOF1 (58% of total variance) at the point A_{WJ}. (c) As (b), except for the last eight-year period of the EOF1. The EEMD is then applied to the EOF temporal structure to decompose temporal variability: (d) intraseasonal, (e) semiannual (f) annual, and (g) interannual variabilities with their corresponding red spectrum as a reference for 95% confidence limit (left panel), whereas (h) represents the long-term trend.

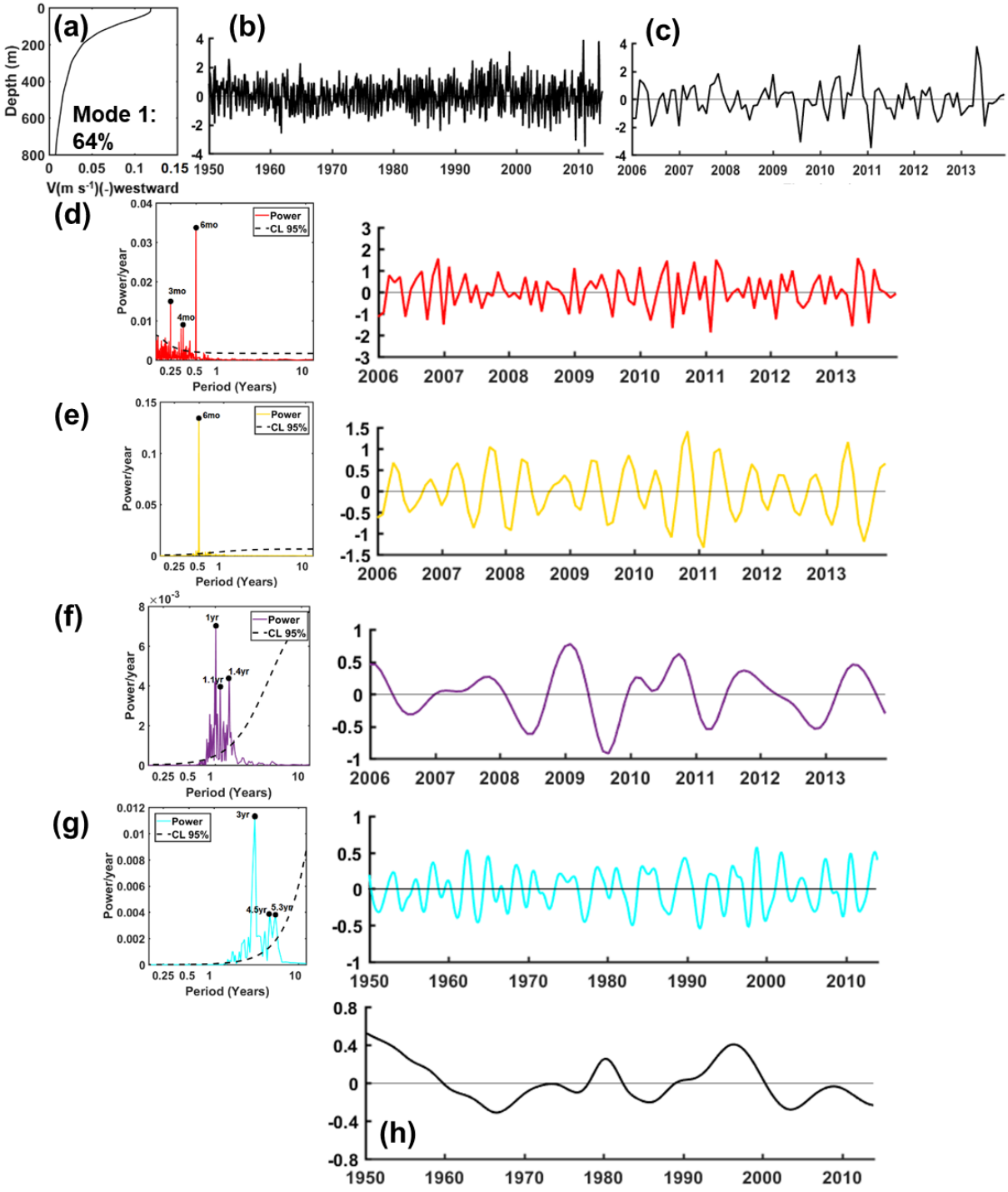

Figure 6. Same as in Figure 5, except for the point B_{SM} with the temporal variability of EOF1 accounting for 64% of total variance.

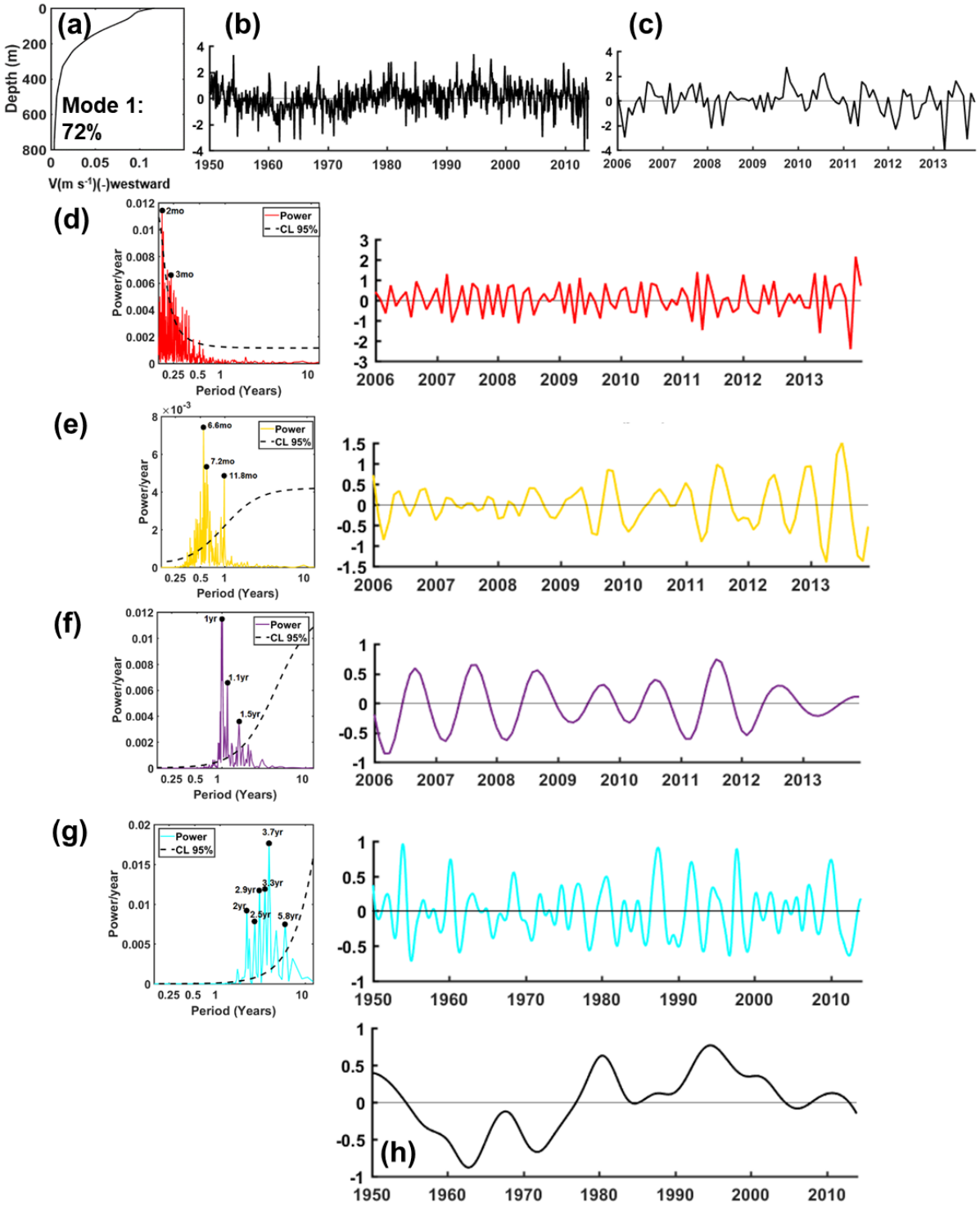

Figure 7. Same as in Figure 5, except for the point C_{EJ} with the temporal variability of EOF1 accounting for 72% of total variance.

Minor comments:

1. This study investigates the variability of zonal current in the Southeastern Tropical Indian Ocean using HYCOM simulations. Hence, the characteristics described in the manuscript might be depended on the model. The authors may moderately change the title, for example, "Simulated Zonal Current Characteristics in the Southeastern Tropical Indian Ocean (SETIO)".

Thank you for your suggestions. As suggested by the reviewer, we have changed the title to "Simulated Zonal Current Characteristics in the Southeastern Tropical Indian Ocean (SETIO)".

2. Line 40-45: I do not understand the logical relationship here between previous studies and what you said after "Hence". What is the scientific question that is not understood in previous studies and what is your purpose? That should specified clearly and unambiguously.

Thank you very much for the careful reading of our manuscript. To make it more obvious and easier to understand the narration, we have reorganized the description, as follow:

Regarding dynamics and characteristics of the SETIO, especially adjacent to the western coast of Sumatra and the southern coast of Java, all previous investigations are either based on numerical model, remote sensed data or velocity/moorings observations within the Indonesian seas or at the exit passages of Indonesian seas (Sunda, Lombok, Ombai, and Timor passages) which lead into the SETIO. There is almost no ocean current/velocity measurement within the SETIO. The observational velocity data are available only at limited points in space and time. The only velocity measurement in south of Java or in the SETIO region reported by Sprintall et al. (1999). The mooring was deployed south of Java in 200 m water depth from March 1997 to March 1998 at depths of 55 m, 115 m and 175 m velocity measurements, but only current meters at 115 m and 175 m were fully working properly (Sprintall et al., 1999). Recently, there are some moorings to measure velocity and stratification deployed in the SETIO region. However, they have not been fully recovered nor published. Hence, due to limited in situ velocity measurements in the SETIO, the detailed dynamics and characteristics of ocean currents in the region have not been fully explained. It is important to obtain a better understanding of current characteristics as well as their spatial and temporal variations in the SETIO adjacent to the southern coasts of Sumatra and Java both for scientific and practical reasons, such as fisheries, climate, and navigation. These are the main motivations of the present study.

3. Line 47: "have been carried out by previous investigators" -> have been investigated

Thank you very much for your correction. We have changed "have been carried out" to "have been investigated".

4. Lines 65-70: The authors may also review the salinity effect in the inter-annual and decadal variability of ITF. For example, Hu and Sprintall 2016, JGR; 2017, GRL; Jyoti et al., 2019. The salinity effect mechanism is an important component of ITF dynamics different from the wind forcing mechanism.

Thank you very much for your suggestion. We have added the review of the salinity effect in the inter-annual and decadal variability of ITF as suggested by the reviewer, as follow:

In addition to the wind forcing mechanism, fluctuations in rainfall over the Indonesian Seas that modulates salinity also influences the ITF transport on interannual (Hu and Sprintall, 2016) and decadal (Hu and Sprintall, 2017; Jyoti et al., 2019) time scales. They found that the salinity effect mechanism is an important component of ITF dynamics and it is different from the wind forcing mechanism. Moreover, it has been revealed that salinity effect contributes 36% of the total interannual variability of the ITF transport (Hu and Sprintall, 2016) and

dominates an increasing trend of the ITF transport during the past decade (Hu and Sprintall, 2017).

5. Line 100: Does the HYCOM assimilate surface observations?

Yes, the HYCOM assimilates surface skin temperatures from NCEP Reanalysis Data (4 times daily).

6. Lines 132-133: No necessary to repeat the references of EEMD here

Thank you very much for your correction. We have deleted the references of EEMD.

7. Section 3.1: A longitude-depth plot of mean zonal currents along the three sections should be presented.

Thank you very much for your suggestion. We have added a longitude-depth plot of mean zonal currents along the three sections (Fig. 8) and additional description of it, as follow:

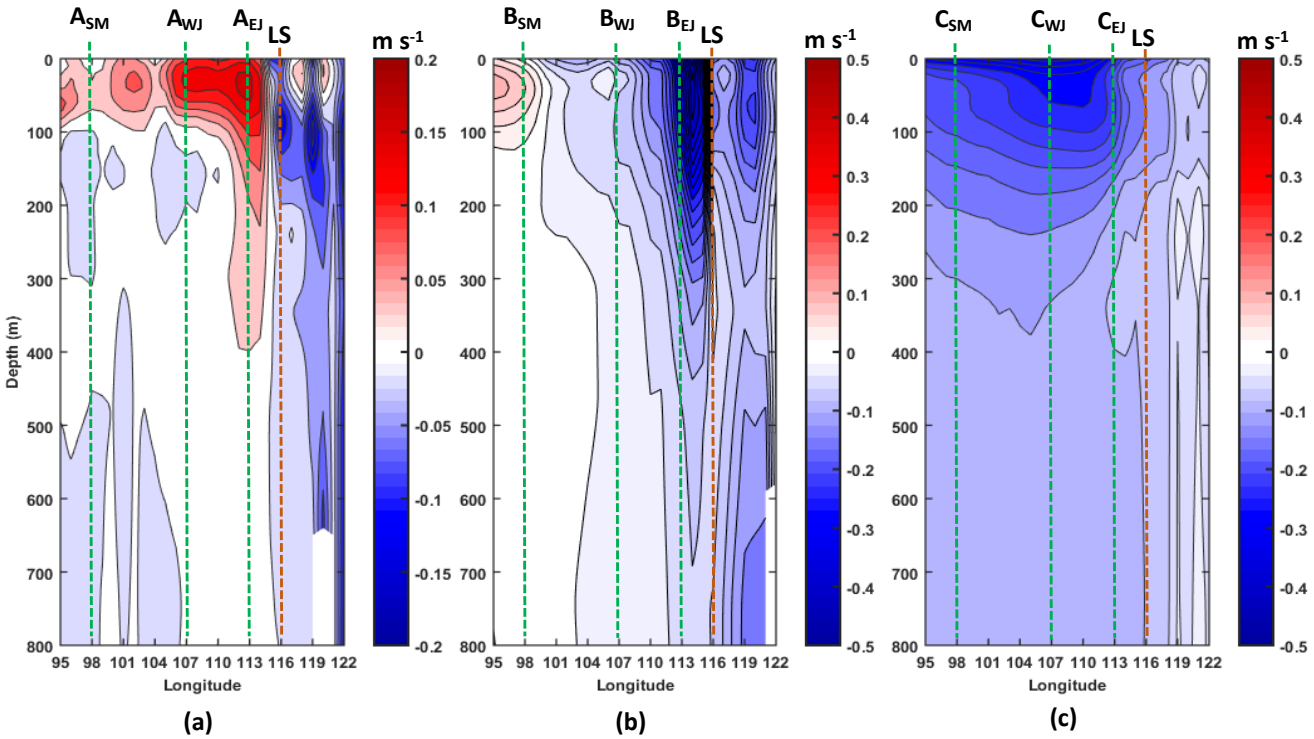

Figure 8. Longitude-depth profiles of mean zonal currents along (a) Transect A, (b) Transect B, and (c) Transect C. Positive (negative) values of the zonal currents indicate eastward (westward). Green dash lines denote longitudes of the nine selected points, whereas dark orange dash lines denote longitude of Lombok Strait (LS).

Here, longitude-depth plots of mean zonal currents along the sections A, B, and C are also presented in Fig. 8, which clearly shows different zonal current system along the transects. Mean zonal currents along Transect A (Fig. 8a) show two distinctive features: (1) the mean currents dominantly flow eastward from the sea surface to 100 m depth (95° E–114° E), and (2) they are predominantly westward from the region (115° E), which is close to Lombok Strait (LS) as one of the ITF exit passages, to the 122° E longitude line. In addition, the mean

eastward current at A_{EJ} occurs up to ~600 m. Meanwhile, the average current on Transect B (the transitional zone) is westward, especially at longitudes 101° E to 107° E (Fig. 8b). In the offshore region (Transect C), mean zonal current flows westward throughout the region (Fig. 8c).

= = = = = = = = = = = = = = = = = =

Revision of Major comments # 1: description revision of "Vertical structure of zonal current" in sections 3.2.1, 3.2.2 and 3.2.3 by using meridional sections.

3.2.1 Vertical Structure of Zonal Current along Meridional Section East Java (A_{EJ}-B_{EJ}-C_{EJ})

Different zonal current system along the meridional transect East Java (EJ; A_{EJ}-B_{EJ}-C_{EJ}) can clearly be seen in Figs. 3a-f. On average, for the period 1950 through 2013, zonal climatological current at A_{EJ} (nearshore area) generally flows eastward from the sea surface to 100 m depth (Figs. 3a and 3d) and reaches its maximum value of about 0.16 m s^{-1}. It is suggested that the average zonal current at this point is mainly attributed to SJC and it shows seasonal variations. During the SE monsoon (JJA), the strength of climatological eastward SJC at this point in upper 10 m depth reduces (Figs. 3d). Meanwhile, during the NW monsoon (DJF), the current in the upper 10 m (Figs. 3d) flows more eastward in response to the prevailing northwesterly winds (Fig. 9). In general, the mean eastward current at A_{EJ}, during DJF was attributed to winds. Interestingly, however, the eastward current occurs up to ~800 m. Other physical processes may account for the eastward current at A_{EJ}, particularly that at depth beneath 100 m. The SJC and SJUC are defined as the surface current in the upper 150 m and the subsurface current beneath 150 m down to 1000 m, respectively (Iskandar et al., 2006) and they are attributed to the arrival of a downwelling Kelvin wave at the south coast of Java (e.g., Sprintall et al., 1999, 2000; Iskandar et al., 2006). Downwelling Kelvin waves originating in the equatorial Indian Ocean during the transitional monsoons propagate along the coasts of western Sumatra and southern Java with phase speeds ranging from 1.5 to 2.9 m s^{-1} (e.g., Sprintall et al., 2000; Syamsudin et al., 2004; Iskandar et al., 2005). These phase speeds indicate that the downwelling Kelvin waves will arrive at A_{EJ} in 21 – 41 days. In this case, downwelling Kelvin waves generated during the monsoon transition period in November may arrive at A_{EJ} in December/January. Therefore, in addition to the local eastward winds, the downwelling Kelvin waves may also contribute to the eastward currents at A_{EJ} during the NW monsoon, including those at depth beneath 100 m.

Meanwhile, the average current at B_{EJ} (the transitional zone) is westward. It is suggested that the mean westward current at the point B_{EJ} is more dominated by the ITF (shown by black lines in Figs. 3b and 3e). Based on observation in the exit passages (Lombok Strait, Timor Passage, and total ITF along exit passages), ITF in JJA is stronger than that in DJF (e.g., Sprintall et al., 2009). In this study, however, it is found that westward current at the point B_{EJ} at 100 m depth is stronger during DJF than JJA. This phase changing (delay) of the ITF seasonality from JJA to DJF at this point is also found in the Ombai Strait as documented by Sprintall et al. (2009, their Table 3; 2010, their Fig. 3). Moreover, Sprintall et al. (2010) found cores of subsurface maximum ITF during DJF extending from 100–250 m (100–800 m) depth at the northern (southern) part of the strait. In this study, this seasonal feature of the subsurface maximum ITF is also found at B_{EJ} in which the corresponding westward current at this point reaches its maximum values at ~100 m depth and the maximum westward current is stronger during DJF than JJA (Figs. 3b and 3e). Hence, we suggest that the primary driver for zonal

westward current at B_{EJ} is the ITF coming from the southern Ombai Strait. To confirm the above relation, we have calculated the correlation between zonal westward current at a depth of ~100 m at point B_{EJ} and that representing subsurface (~200 m) maximum ITF in the southern Ombai Strait (Sprintall et al., 2010). The correlation coefficient between the zonal westward current at ~100 m at the B_{EJ} and that of the southern Ombai Strait is 0.58 with the 95% significance level approximately ±0.33. This study shows that the zonal westward current at 100 m depth at B_{EJ} has a strong correlation with the subsurface (~200 m) maximum ITF in the southern Ombai Strait, confirming that the ITF flowing from the Ombai Strait is the primary driver for zonal westward current at B_{EJ}.

In the offshore region of the study area, zonal current at C_{EJ} (Figs. 3c and 3f) flows westward throughout the year and has average velocity around 0.20 m s^{-1} in the upper 100 m. Under such characteristics we supposed that the westward current at this point is the SEC in the southeast Indian Ocean, which joins the ITF flowing out from the Lombok and Ombai Straits, and Timor Passage. The HYCOM westward current at this point is stronger during JJA than DJF, which is associated with seasonal characteristics of the ITF in Lombok Strait, Timor Passage, and of the total ITF through the Lombok and Ombai Straits, and Timor Passage (Potemra, 1999; Sprintall et al., 2009). The westward current at C_{EJ} (Figs. 3c and 3f) reaches its maximum value of about 0.31 m s^{-1}.

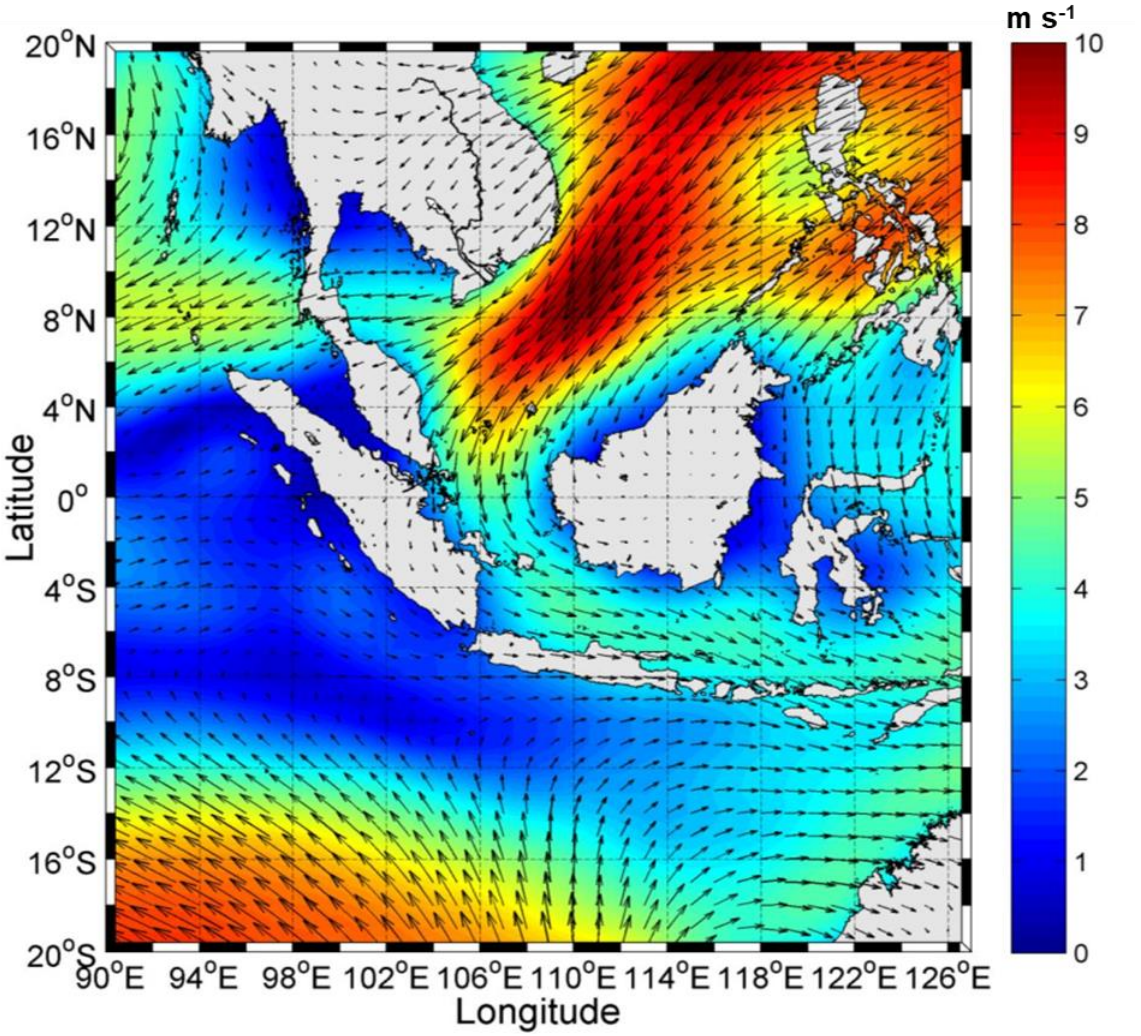

Figure 9. Mean NW monsoon for the period of 1950 to 2013 (climatological wind field during the DJF).

3.2.2 Vertical Structure of Zonal Current along Meridional Section West Java (A_{WJ}-B_{WJ}-C_{WJ})

Figures 3g-l show vertical structure of zonal current along the meridional transect West Java (WJ; A_{WJ}-B_{WJ}-C_{WJ}). Similar to A_{EJ}, mean zonal current at A_{WJ} (nearshore region) is attributed to SJC, which generally flows eastward in upper 100 m depth (Figs. 3g and 3j) and reaches its maximum value of about 0.12 m s^{-1}. Our simulation shows that during the monsoon transitions (MAM and SON), SJC is eastward and intensified by the propagation of coastal Kelvin waves associated with the Wyrtki Jet in the equatorial Indian Ocean, which is forced by the local equatorial zonal winds during both monsoons. These waves propagate along the Sumatra-Java coast (i.e., Sprintall et al., 2000; Druskha et al. 2010, Iskandar et al. 2009) and some portions propagate northward into the Lombok and Makassar Straits (Susanto et al., 2000; 2012; Pujiana et al., 2013), whereas the remaining parts continue eastward (Syamsuddin et al., 2004). Furthermore, the present study shows that the eastward current during SON is stronger than that during MAM, which is consistent with mooring observation in the Makassar Strait (Susanto et al., 2012; their Fig. 3). The stronger eastward current during SON was supposed to be attributed to the faster and more intense climatological Wyrtki Jet during SON than that during MAM (Knox, 1976; McPhaden, 1982; Han et al., 1999; Qiu et al., 2009; McPhaden et al., 2015; Figs. 1d and 2e of Duan et al., 2016) and also associated with the stronger wind forcing over the eastern equatorial Indian Ocean during the SON compared with the MAM period (figure not shown), which is responsible for the Jet.

Moreover, it can be seen that during the NW monsoon the eastward current at A_{WJ} (Figs. 3g and 3j) is weaker than that at A_{EJ} (Figs. 3a and 3d). The weaker current at A_{WJ} may exist as a consequence of the weaker mean NW monsoon at this point compared with that at A_{EJ} (Fig. 9). Interestingly, at a depth of 100 m, there is a maximum westward current at A_{WJ} during DJF with velocity of about 0.1 m s^{-1} (Figs. 3g and 3j). Here, we suggest that ITF is the cause of the westward current at 100 m at A_{WJ} during the DJF. In regard to the ITF, Fig. 3 of Sprintall et al. (2010) shows cores of subsurface maximum ITF extending from 100 m to 250 m depth in the northern part of the Ombai Strait and from 100 m to 800 m depth at the southern part of the strait during DJF. Meanwhile, the influence of ITF on the zonal current at A_{EJ} at 100 m is weaker as a consequence of the stronger NW monsoon at A_{EJ} compared with those at A_{WJ} (Fig. 9), so that the current flows rather eastward at A_{EJ} during DJF (Figs. 3a and 3d).

To further investigate which one is more influential between the ITF and the NW monsoon to force the zonal current at the A_{WJ} and A_{EJ} at 100 m depth, we have carried out correlation between the zonal current at both points (each at depth of ~100 m) and each the NW zonal wind and the zonal current representing subsurface (~200 m) maximum ITF in the southern Ombai Strait (Table 2). Here, the ITF in the southern part of the Ombai Strait was chosen for carrying out the correlation because the ITF flows mainly through the southern part of the passage (Sprintall et al., 2010). It is found that the subsurface maximum ITF during DJF exists at a depth of about 200 m in both the northern and southern parts of the Ombai Strait and it is stronger during DJF than JJA in both parts of the strait (Fig. 3 of Sprintall et al., 2010). In this study, the DJF zonal currents in the period of 2004 through 2006 in the southern Ombai Strait derived from the INSTANT program (http://www.marine.csiro.au/~cow074/ instantdata.htm) were used for the correlation analysis.

It is found that during DJF the zonal current at A_{WJ} at 100 m shows high correlation with the subsurface (~200 m) maximum ITF in the southern Ombai Strait, whereas its correlation with

the NW zonal wind is weak (Table 2). Moreover, although during DJF the correlations between the zonal current at A_{EJ} at 100 m and each NW zonal wind and subsurface (~200 m) maximum ITF in the southern Ombai Strait are below the significance level, the NW zonal wind is more influential to force variation of zonal current at A_{EJ} at 100 m than the ITF. Hence, during DJF we suggest that the westward current simulated at A_{WJ} at 100 m is ITF-related, whereas that at A_{EJ} is relatively NW zonal wind-related. As already discussed, in addition to the local eastward winds during DJF, it is suggested that the arrival of downwelling Kelvin waves in December/January at A_{EJ} may contribute to a net eastward current across the water column, which in turn reducing the influence of ITF at this point.

Table 2. Correlation coefficients between zonal currents at 100 m depth at both AWJ and AEJ and each the local NW zonal wind and subsurface (200 m) maximum ITF in the southern Ombai Strait during DJF in the period of 2004 through 2006.

Points	**Correlation Coefficients (*r*)**[a)]	
	***U*-SMITF**	***U*-NWZW**
A_{WJ}	0.76	-0.32[b)]
A_{EJ}	-0.13[b)]	0.30[b)]

[a)] The 95% significance level is approximately ± 0.33. *U*: zonal currents at 100 m depth; SMITF: subsurface (200 m) maximum ITF in the southern Ombai Strait; NWZW: northwesterly zonal wind.

[b)] Correlation below the significance level.

In the transition region, the mean current at B_{WJ} is westward and it is more dominated by the ITF (denoted by black lines in Figs. 3g-l). Similar to B_{EJ}, the seasonal feature of the subsurface maximum ITF is also found at B_{WJ} in which the corresponding westward currents at this point reaches its maximum value at ~100 m depth and it is stronger during DJF than JJA and (Figs. 3h and 3k). In this study, it is also found that the zonal westward currents at 100 m depth at B_{WJ} has a strong correlation with the subsurface (~200 m) maximum ITF in the southern Ombai Strait, with correlation coefficient about 0.77 and with the 95% significance level approximately ±0.33, corroborating that the ITF flowing from the Ombai Strait is the main driver for zonal westward current at this point.

Furthermore, like C_{EJ}, characteristic of persistent westward current exists in the offshore region (C_{WJ}), which is attributed to SEC and the westward current has mean velocity around 0.22–0.33 m s^{-1} in the upper 100 m (Figs. 3i and 3l). The simulated westward current at C_{WJ} shows seasonal variations and reaches its maximum value of about 0.48 m s^{-1}.

3.2.3 Vertical Structure of Zonal Current along Meridional Section Sumatra (A_{SM}-B_{SM}-C_{SM})

Vertical structures of zonal current along the meridional transect Sumatra (SM; A_{SM}-B_{SM}-C_{SM}) are shown in Figs. 3m-r. Similar to A_{EJ} and A_{WJ}, mean zonal current at A_{SM} (nearshore region) is eastward, attributed to SJC, and associated with the Kelvin wave propagation. However, due to A_{SM} located in front of west of Sumatra Island (Fig. 2), which is oriented in the northwest-southeast direction, the meridional components of velocity at this point is also dominant (Figs. 1a and 2). Therefore, zonal currents at A_{SM} are relatively weaker than those at A_{WJ} and A_{EJ}, which are located in front of south of Java Island oriented in the west-east direction. For example, during SON, the eastward current reaches its maximum velocity of

about 0.05 m s^{-1} at A_{SM} (cyan lines in Figs. 3m and 3p), whereas it is about 0.23 m s^{-1} (at A_{WJ}; Figs. 3g and 3j) and 0.20 m s^{-1} (at A_{EJ}; Figs. 3a and 3d) at ~30-50 m depths.

Furthermore, results of this study show that a maximum value of the eastward current forced by a Kelvin wave at A_{SM}, A_{WJ}, and A_{EJ} is found at a certain depth (at ~30-50 m depths) and it is supposed to be attributed to a baroclinic Kelvin wave. The baroclinic Kelvin wave propagating vertically and horizontally along its waveguide can exert energy the most at a certain depth (Drushka et al., 2010; Pujiana et al., 2013; Iskandar et al., 2014). According to laboratory experiment observation conducted by Codiga et al. (1999) and Hallock et al. (2009), Kelvin wave can be trapped in a slope and propagates along an isobath. This phenomenon is known as slope-trapped baroclinic Kelvin wave. Moreover, Kelvin wave which propagates along continental slope with strong stratification can cause strong current velocity. Codiga et al. (1999) also found that this slope Kelvin wave is formed after encountering a canyon-like bathymetry. Meanwhile, Pujiana et al. (2013) shows that Kelvin wave propagation from Lombok Strait to Makassar Strait, across Sunda continental slope, is along isobaths at depths greater than 50 m. In this present study, eastward current along the Transect A has maximum current velocity at depth ~30–50 m. Therefore, it is suggested that this maximum eastward current at ~30–50 m depth associated with slope-trapped Kelvin wave, which propagates at that depth along the southern coasts of Sumatra and Java.

In the transition region, characteristic of average zonal current (the climatological current field) at B_{SM} (Figs. 3n and 3q) is different from that at B_{WJ} (Figs. 3h and 3k) and B_{EJ} (Figs. 3b and 3e). The average current at B_{SM} is eastward, while at points B_{WJ} and B_{EJ} it is westward. During NW and transitional periods of the monsoon, zonal current at B_{SM} flows eastward and reaches its maximum velocity of about 0.12 m s^{-1} at a depth of 40 m within the period of SON (Fig. 3q). Meanwhile, during SE monsoon, the zonal current at this point flows westward. In contrast to the mean zonal currents in the nearshore region (A_{SM}), it seems that the average zonal current field at B_{SM} is not attributed to SJC. The reason is the B_{SM} location, which is far from the coasts of Mentawai Islands and Enggano Island off the western coast of Sumatra by 430 km. This distance is more than Rossby radius of deformation at this latitude (~90 km). Thereby, Kelvin waves, which affect the SJC variations, do not exist at this point. We suggest that the current variability at B_{SM} is influenced by tropical current systems in the Indian Ocean, such as the Equatorial Counter Current (ECC), Southwest Monsoon Current (SWMC), and Wyrtki Jet. Here, we displayed seasonal averaged surface currents over 64 years (1950–2013) and schematics of the tropical current systems in the Indian Ocean as supporting evidence (Fig. 10).

Figure 10 shows that B_{SM} is located at an area, which is affected by the ECC, SWMC, and Wyrtki Jet. It can be seen in the Fig. 10a that during DJF, surface currents along the equatorial Indian Ocean is dominated by the westward North Equatorial Current (NEC) and the eastward ECC. Meanwhile, during JJA (Fig. 10c), the NEC disappears and the ECC becomes absorbed into the SWMC, which dominantly flows eastward in the northern Indian Ocean (Tomczak and Godfrey, 1994). In addition, during the transitional periods (MAM and SON), the Jet is generated, and it causes a strengthening of eastward flows along the equatorial Indian Ocean (Figs. 10b and 10d). This explains the cause of climatological current at B_{SM} flows eastward and reaches its maximum velocity during SON and MAM. These currents (the ECC, SWMC, and Wyrtki Jet) flow eastward before they turn and some part of their flow feed into the SEC in the southern Indian Ocean.

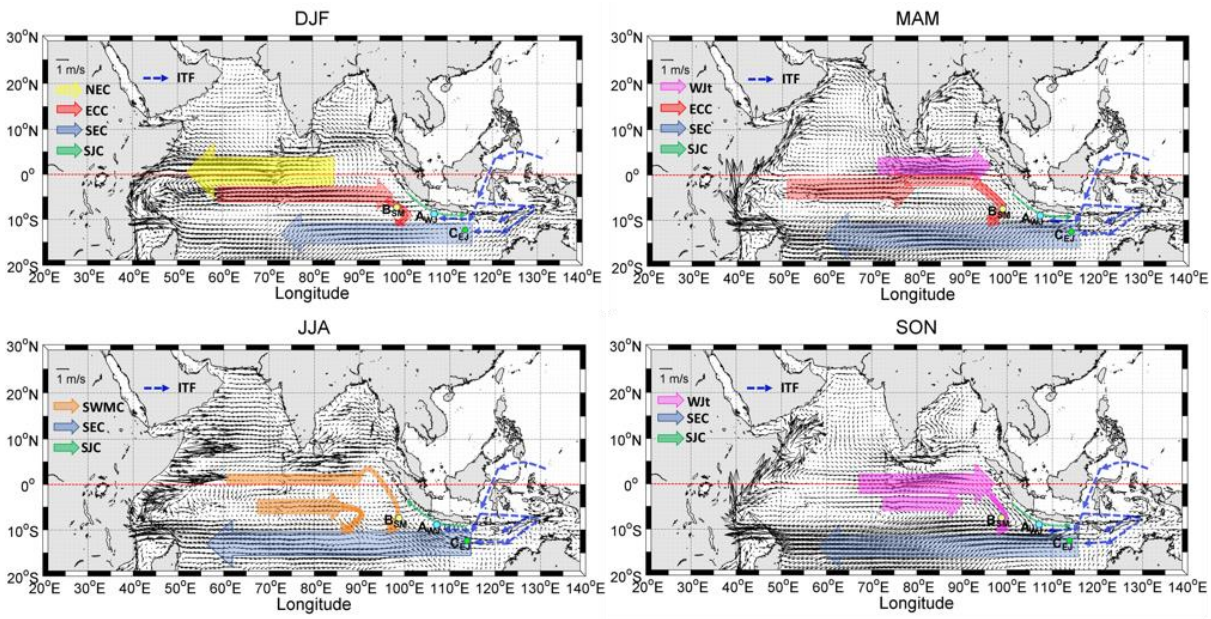

Figure 10. Seasonal averaged surface (1 m) currents over 64 years (1950-2013) and schematics of the tropical current systems in the Indian Ocean during (a) DJF, (b) MAM, (c) JJA, and (d) SON. Current branches indicated by colour arrows (not black) are the North Equatorial Current (NEC), Equatorial Counter Current (ECC), South Equatorial Current (SEC), South Java Current (SJC), Wyrtki Jet (WJt), South West Monsoon Current (SWMC), and Indonesian Throughflow (ITF). The dashed line represents thermocline current.

Current characteristics in the offshore region (C_{SM}) generally show similarities with those at C_{WJ} and C_{EJ}, as shown in Figs. 3o and 3r. The current at C_{SM} is attributed to SEC and flows westward all year round, with mean velocity around 0.18–0.3 m s^{-1} in the upper 100 m. In addition, the strength of westward current at C_{SM} varies seasonally and reaches its maximum value of about 0.42 m s^{-1} during SON (Fig. 3r).